Deep-Sea Research, 1974, Vol. 21, pp. 989 to 1016. Pergamon Press. Printed in Great Britain.

Wave directional spectra from synthetic aperture observations of radio scatter

G. L. TYLER,* C. C. TEAGUE,* R. H. STEWART,†
A. M. PETERSON,* W. H. MUNK† and J. W. JOY†

(*Received* 27 *December* 1973; *in revised form* 18 *April* 1974; *accepted* 18 *April* 1974)

Abstract—We have measured the directional distribution of waves produced by a quasi-stationary, homogeneous wind field. This was done by observing radio backscatter from the LORAN A transmitter on Wake Island. The LORAN frequency of 2 MHz is in Bragg resonance with 7^s ocean waves. A directional resolution of $\pm 3°$ has been attained from a synthesized antenna formed by moving the receiver at constant speed along the airport taxiway. The directional distribution of the 7^s ocean waves as inferred from the variable scatter cross-section compared favorably with directional moments measured with a pitch-and-roll buoy. The directional wave energy is found to fall off monotonically with angle θ relative to the wind, in accord with a model $\cos^S(\frac{1}{2}\theta)$ proposed by LONGUET-HIGGINS, CARTWRIGHT and SMITH, *Ocean wave spectra*, pp. 111–136, Prentice-Hall (1963); s increases with wind speed and decreases with frequency, and can be plotted against a single parameter $\mu = \mu_*/c\kappa$, where $\sqrt{(u_*/\rho)}$ is wind stress, c is phase velocity, and $\kappa = 0{\cdot}4$ is von Karman's constant. The radio measurements give an upper limit of 0·02 for the upwind/downwind ratio in wave energy flux. The ratio of up-down to cross-wind components in mean-square slope computed for the $\cos^S(\frac{1}{2}\theta)$ model is compared to the ratio inferred from measurements of sun glitter. The (second-order) mean-square pressure fluctuations at great depth are computed from our estimates of oppositely traveling wave energy.

1. INTRODUCTION

ARTHUR (1949) first noticed that waves emerge from a fetch with a broad spread in direction, up to $\theta = \pm 45°$ relative to the mean wind. Accordingly, he suggested tha the generated wave *height* be taken to vary as $\cos\theta$. In a more precise formulation PIERSON, NEUMANN and JAMES (1955) (PNJ) proposed the frequency-directional energy spectrum $F(\omega, \theta) = \varphi(\omega)\, 2\pi^{-1}\, g(\theta)$, with

$$g(\theta) = \cos^2\theta, \quad -\tfrac{1}{2}\pi \leq \theta \leq \tfrac{1}{2}\pi$$
$$= 0 \text{ otherwise.} \tag{1.1}$$

The PNJ spectrum has been used faithfully by a generation of oceanographers. KINSMAN (1965, p. 399) has this to say: "So long as you don't do something absolutely absurd, you are bound to get 'oceanographic level' agreement. Some day somebody is going to take a close, accurate look, and the whole 'agreement' will go sky high."

An ambitious effort to get better information resulted in the Stereo Wave Observation Project (SWOP); at 1700 Z on 25 October 1954, in the North Atlantic, about 100 stereo photographs of the ocean surface were taken. After a 3-year effort involving a number of organisations, two of the stereo pairs were finally combined to produce the first wavenumber energy spectrum (CHASE, COTE, MARKS, MEHR, PIERSON, RÖNNE, STEPHENSON, VETTER and WALDEN, 1957). "... I doubt that it will ever become habit forming", wrote Kinsman. On the basis of SWOP it was proposed that equation

*Center for Radar Astronomy, Stanford University, Palo Alto, Calif., U.S.A.
†Scripps Institution of Oceanography, University of California, La Jolla, Calif. 92037, U.S.A.

(1) be extended by a frequency-dependent term proportional to $\cos^4\theta$; the result of this modification was to make the angular pattern somewhat frequency-dependent, with wider spread at higher frequency. Other optical investigations have followed. Cox and Munk (1954a, b) derived some *gross* directional properties from aerial photographs of sun glitter. Stilwell (1969) and Sugimori (1973) were able to obtain *spectral* properties from photographs of the sea surface outside the glitter, using the continuous skylight rather than the sun for illumination. The method for obtaining Fourier transforms follows a pioneering suggestion by Barber (1949).

A substantial advance was made by Longuet-Higgins, Cartwright and Smith (1963) (henceforth LCS) and by Cartwright (1963). Using the measured tilt and acceleration of a floating buoy, LCS suggested a directional pattern

$$g(\theta) = \cos^s(\tfrac{1}{2}\theta), \quad -\pi \leq \theta \leq \pi, \quad s = s(\omega), \tag{1.2}$$

with s near 1 at high frequencies, increasing to near 10 at low frequencies.* Subsequent measurements by Ewing (1969) have confirmed this general pattern.

In the present experiment the directional characteristics of ocean waves were obtained from backscattered 2 MHz radio waves transmitted and received on Wake Island. The measurements are consistent with a minor modification of the LCS pattern,

$$G(\theta) = \alpha + (1-\alpha)\cos^s(\tfrac{1}{2}\theta), \quad -\pi \leq \theta \leq \pi, \tag{1.3}$$

allowing for a slight energy flux, α, opposite the prevailing winds.

Radio waves in the 2–30 MHz frequency band (commonly called HF or decameter waves) are well suited to ocean wave studies; the interpretation is straightforward in terms of (first-order) Bragg theory (Barrick, 1972), and the Bragg-selected wavelength covers the energetic band of the ocean wave spectrum (2- to 7-s periods). The predictions of the theory have been verified to high precision in an experiment by Crombie (1955). With modern equipment the Bragg signal may be detected at signal-to-noise ratios in excess of 40 dB. Our work is a simple modification of the Crombie experiment (a moving receiver), taking advantage of the very high signal-to-noise ratio.

The radio technique described below provides 360° coverage for waves coming toward the island and for waves receding from the island. Here we are concerned with approaching waves only. The receding waves will be separately discussed; they lie in the island shadow and give information on regeneration over limited fetches.

The purpose of the Wake Island experiment is threefold: (i) to compare the radio-scatter cross-sections with wave measurements from a floating buoy, thus testing the assumptions of homogeneity and the applicability of first-order Bragg mechanism; (ii) to measure directional wave spectra to an angular resolution about 10 times that achieved by previous methods; and (iii) to contribute towards remote sensing of surface wind directions by a comparison of approaching to receding wave energy.

2. RADIO TECHNIQUE

Bragg scatter is a selective, resonant interaction. At grazing incidence a radio wave

*LCS write $g(\theta) = \cos^{2S}(\tfrac{1}{2}\theta)$.

of wavenumber $\vec{k}_r$ is backscattered by an ocean wave propagating radially toward or away from the radio source and having a wavelength one-half the radio wavelength ($\vec{k} = \pm 2\vec{k}_r$). The Doppler shift of the scattered wave is $\pm\omega$ (neglecting currents), where $\omega = (gk)^{\frac{1}{2}}$ is the resonant ocean-wave frequency. *Approaching* ocean waves produce a positive Doppler shift, receding waves a negative Doppler shift. For example, waves traveling north-to-south are seen as approaching waves with an antenna looking northward, and as receding waves with an antenna looking south. By observing positive and negative Dopplers in all directions, one has, in principle, 360° coverage for both approaching waves and receding waves.

The power of the scattered signal varies as $\vec{k}^4 F(\pm 2\vec{k}_r)$, where $F(\vec{k})$ is the ocean-wave spectrum. The intensity of ocean waves approaching from the north is measured in a scattering area north of the island; of waves approaching from the west in an area to the west, etc. We then combine the measured intensities into a directional spectrum, thus assuming that the wave *statistics* are the same whether we look north or west. This assumption of a *homogeneous* wave field is crucial. Sometime in the future we hope to conduct a nonhomogeneous experiment, measuring wave statistics at various distances from the coast in the presence of offshore winds.

Good directional resolution of the wave spectrum calls for a radio antenna many wavelengths long (typically 1 km for the present experiment). Fortunately, a suitable antenna can be synthesized using a coherent transmitter and sampling the received field with a simple antenna carried along a straight line at a constant velocity.* (Neither a straight path nor a constant velocity is necessary if the actual path and velocity are known.)

For a receiver moving at speed v in the direction γ, the radio waves backscattered from a patch centred at r, φ (Fig. 1) are Doppler-shifted by

$$\Delta\omega_r = \pm\omega + vk_r \cos(\varphi - \gamma), \quad \omega^2 = gk, \; k = 2k_r. \tag{2.1}$$

The ($\pm$) sign is associated with (approaching/receding) waves in the patch,

$$\varphi = \mp\beta. \tag{2.2}$$

The problem is to solve for β as a function of $\Delta\omega_r$. To avoid ambiguity in the arccos, it is necessary that

$$v < \omega/k_r = 2\omega/k = 2c,$$

where c is the ocean-wave phase velocity.† The sign in φ–γ is resolved by sequentially sampling two asymmetric antenna elements and solving for the strength of the echoes from the left and right in a least-square sense.

The resolution, $\delta\varphi$, of the synthesized antenna depends on the total distance D

*This technique was first suggested by Barber (1959), who proposed the use of a wire trailed from an airplane.

†In our experiment, $c = 11$ m s^{-1} and $v = 7$ m s^{-1} (26 km h^{-1}).

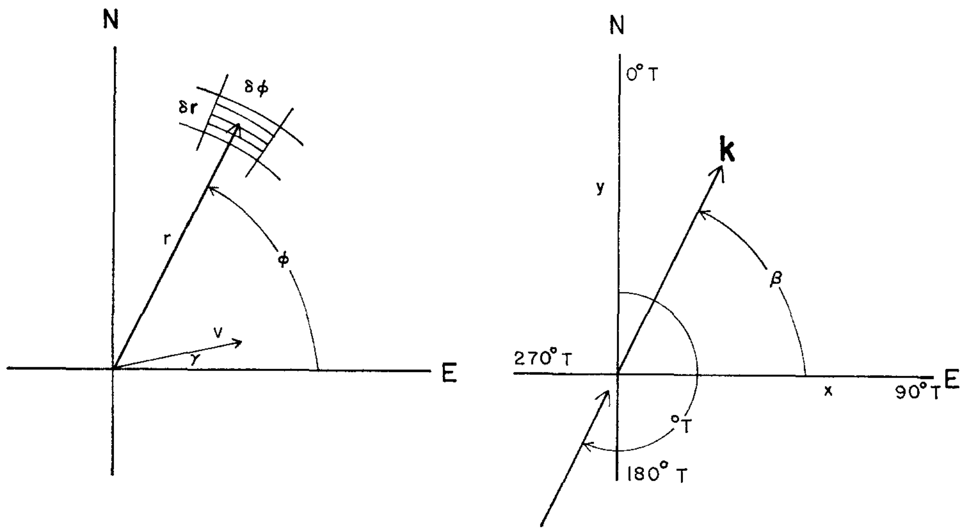

Fig. 1. *Left:* Geometry for synthetic aperture technique. Radio transmitter and receiver are near the origin. The receiver moves with velocity v in the direction γ, receiving backscattered signals from an area $r\delta\varphi.\delta r$ centred at r,φ. Pulse length determines δr, antenna directional resolution determines $\delta\varphi$. *Right:* Directional conventions. Waves travel *towards* β, measured counterclockwise from east (vector convention). Waves come *from* °T, reckoned clockwise from north (wind convention). The relation is $°\mathrm{T} + \beta = -\frac{1}{2}\pi$.

over which the signals are received and the weighting function used in calculating the Doppler spectrum, but it corresponds closely to that of a broadside antenna of length D, i.e.*

$$(\delta\varphi)^{-1} \approx D\tilde{k}_r \sin \mid \varphi_w - \varphi \mid. \tag{2.3}$$

We refer to TEAGUE, TYLER, JOY and STEWART (1973) for further discussion.

A typical Doppler spectrum* for a stationary receiver (Fig. 2) consists of two sharp lines at $\Delta\tilde{\omega}_r = \Delta\omega_r/2\pi$ Hz, $\Delta\omega_r = \pm\sqrt{(gk)}$, corresponding to approaching/receding waves, respectively. (The small bumps at zero and 0·2 Hz are due to second-order scatter.) For a moving receiver the two lines are broadened in accordance with the wave direction [equations (1, 2)]. For example, the upper frequency limit of the positive Doppler band corresponds to approaching waves traveling opposite to the receiver, the lower limit to waves approaching the island traveling in the direction of the receiver. The backscattered power density is proportional to the associated wave spectral density and to the (known) size of the scattering area, and so the Doppler spectrum can be mapped into an ocean-wave directional spectrum.

The radio scatter technique is best suited for measuring the *relative* directional distribution, the scattering area being then the only variable experimental parameter. An absolute measurement of the wave spectrum is much more difficult, requiring an accurate knowledge of radiated power, antenna and receiver gain, and of propagation losses.

*All observations are in *cyclical* frequencies, $\tilde{\omega} = \omega/2\pi$ (Hz), $\tilde{k} = k/2\pi$ (cycles m^{-1}), etc.

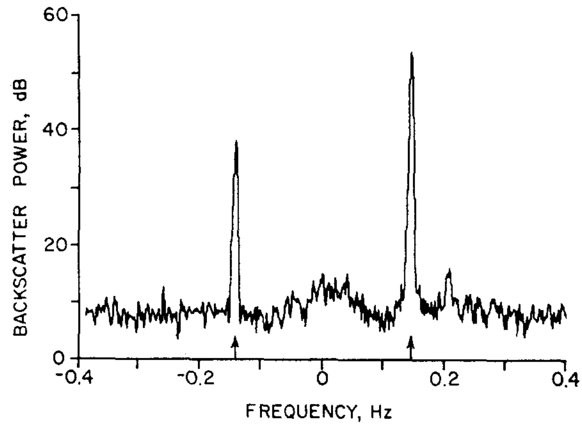

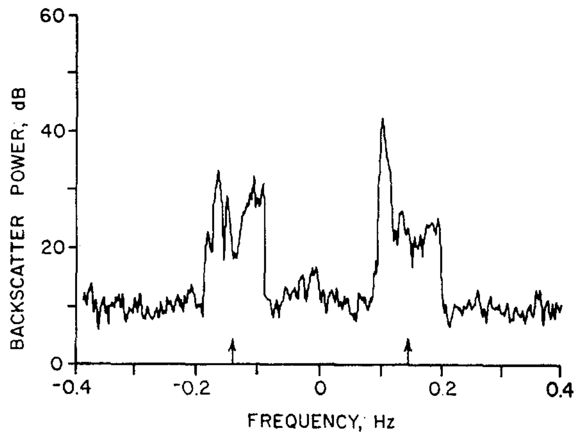

Fig. 2. Doppler spectra of LORAN A radio signals backscattered from an annulus 37·5 km wide, as recorded at Wake Island on 13 November with a stationary receiver (top) and moving receiver (bottom). Arrows at $\pm 0 \cdot 14$ Hz indicate the frequency of the Bragg-selected ocean waves. For the moving receiver the two Doppler lines are spread into a band, in accordance with wave direction relative to the moving receiver.

3. WAVE BUOY

For comparison with the radio scatter observations, simultaneous wave measurements were taken by a wave buoy deployed in the scattering area. The buoy is disc-shaped, follows the water surface, and records vertical accelerations and the two components of tilt. Our buoy is similar to the 'pitch-and-roll buoy' designed at the National Institute of Oceanography* (LONGUET-HIGGINS, CARTWRIGHT and SMITH, 1963) and the wave buoy of the former Hudson Laboratories (SAENGER, 1969).

The buoy is 1·7 m in diameter, weighs 150 kg, and has a draft of 8 cm. An accelerometer is mounted on the axis of a vertical gyro; surface tilts are measured relative to the gyro axis, and buoy heading relative to a gyro-stabilized magnetic compass. The instrument is completely self-contained. Data from the transducers are filtered to reduce aliasing and recorded on computer-compatible magnetic tape to an accuracy of one

*Now Institute of Oceanographic Sciences.

part in 2^{12} (approximately $\pm 0{\cdot}01\,\%$). Typically, 16 10-min segments of data were recorded on each day of operation.

The raw data are Fourier-transformed, and corrections made for filtering, then transformed back into the time domain and the observed tilts rotated to geographical coordinates. A Fourier transform yields the cross-spectral matrix between acceleration and the tilt-components. The acceleration spectrum is multiplied by ω^{-4} to give the elevation spectrum, and the tilts and elevations are corrected for buoy response.

Wave-tank calibrations show a flat heave response up to 0·6 Hz, falling off at higher frequencies (half-power at about 0·7 Hz). The slope response extends to slightly higher frequencies. In general, the observed acceleration spectra have a signal-to-noise ratio better than 1000 : 1, the slope spectra better than 100 : 1 in the interval 0·05–1 Hz. The noise is white, and probably due to the weakly nonlinear response of the buoy. A detailed description of the buoy, transducers, and their calibration is in preparation.

4. WAKE ISLAND EXPERIMENT

The experiment was conducted in November, 1972, on Wake Island (Fig. 3). The island is small and so hardly distorts the radio field. A long runway and several other paved areas are suitable for the synthetic aperture measurements. A LORAN A transmitter serves as a convenient source of high-power coherent radio pulses. Further, uniform wind fields are of common occurrence in this area.

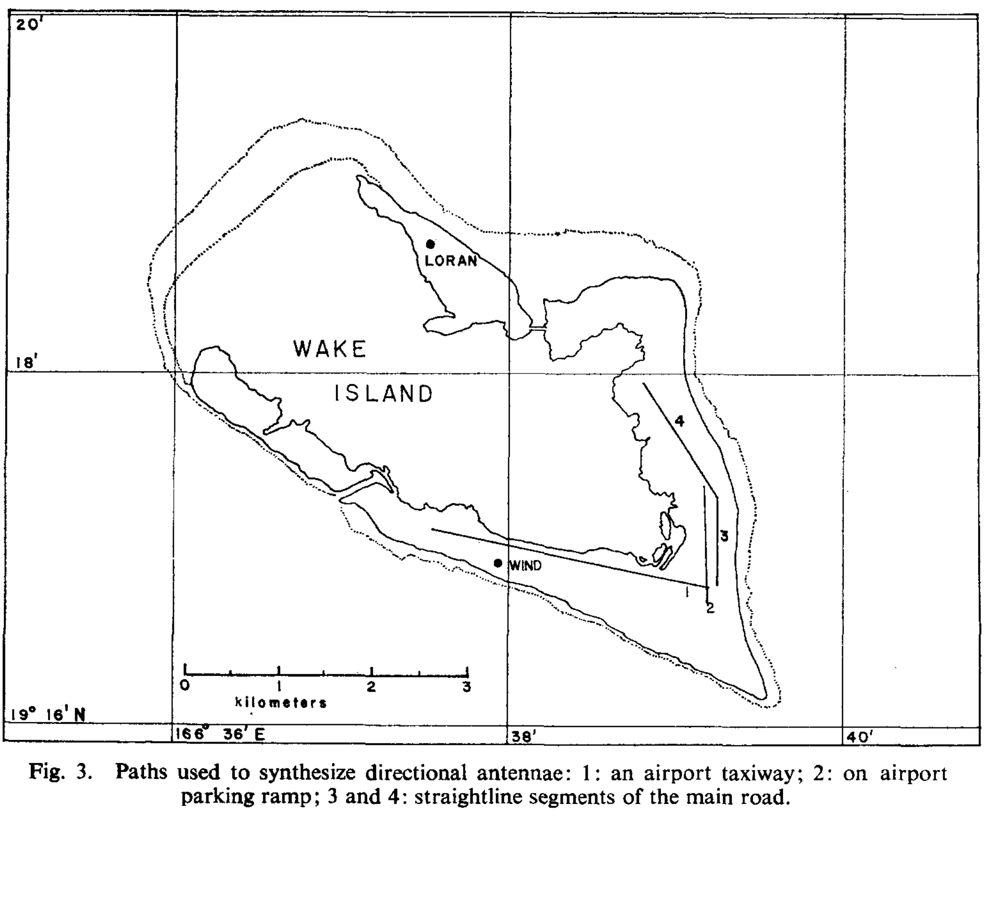

Fig. 3. Paths used to synthesize directional antennae: 1: an airport taxiway; 2: on airport parking ramp; 3 and 4: straightline segments of the main road.

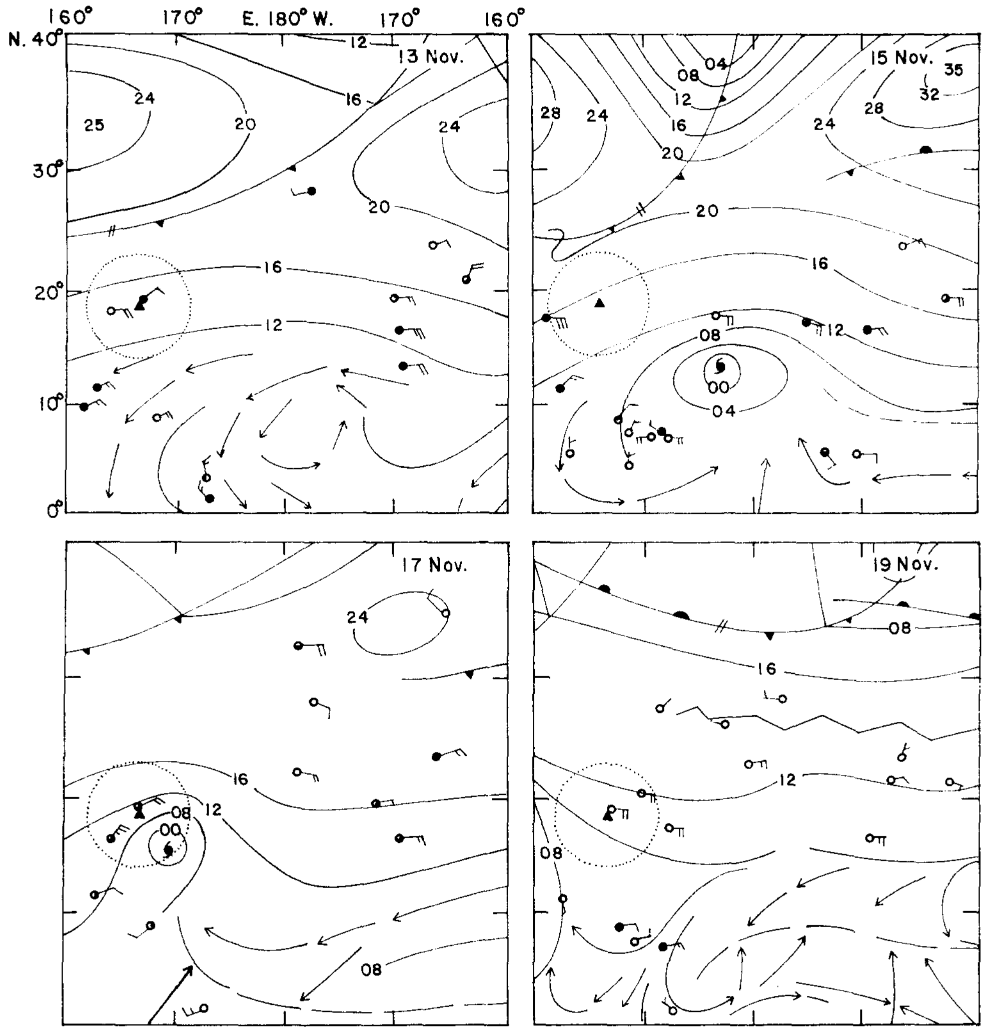

Fig. 4. Synoptic weather maps at local noon (0000 Z) for indicated alternate dates in 1972, abstracted from the Global Tropical Analysis issued by the National Weather Service, NOAA. Pressure contours in mbar relative to 1000 mbar. A ring of 500 km radius is drawn about island (▲).

The radio data were collected for 9 days under very fortunate meteorological conditions (Fig. 4). The weather was dominated by moderate to strong trade winds extending 500–2000 km upwind from the island. On 13 November the winds were associated with a weak front 1000 km to the north and a depression 1500 km to the southeast. The depression became a small typhoon, 'Ruby', which moved toward the island, passing to the south, and quickly dissipated after 18 November. Ruby's primary effect at Wake Island was to strengthen the northeasterly winds for several days, and then shift them to the east.

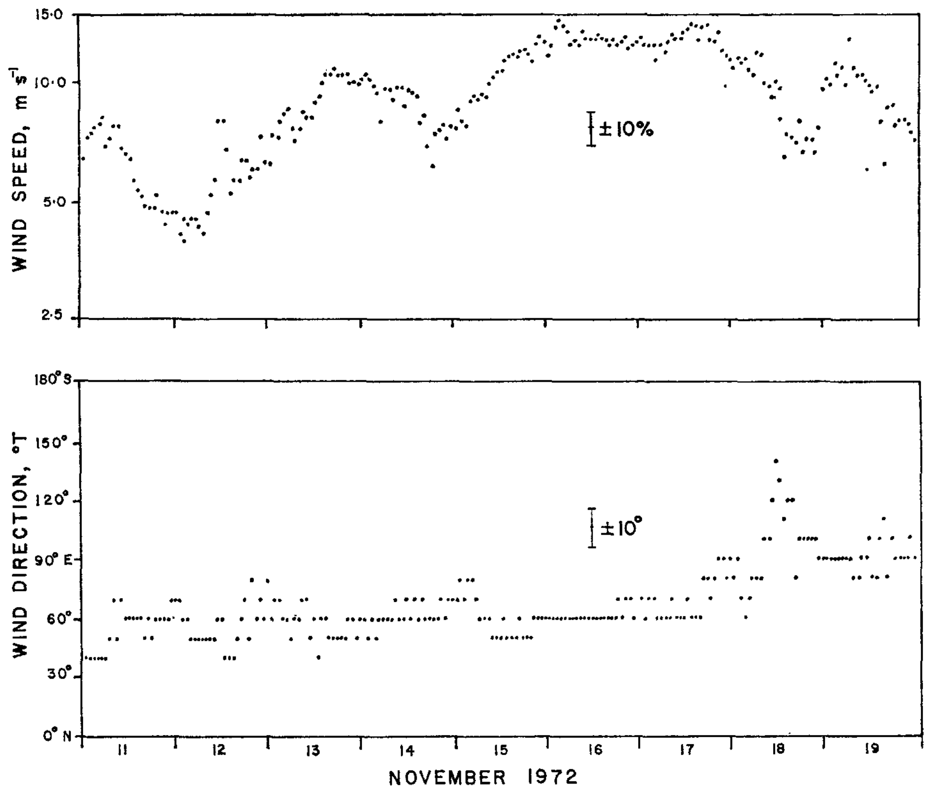

Fig. 5. Hourly averaged wind speed and hourly wind direction at Wake Island weather station. Wind speed is plotted logarithmically to give uniform percentage variability. Vertical tickmarks are local midnight.

Wind direction recorded at the island weather station* (Fig. 5) was between 40° and 80°T from the 11th through the 17th, and within $\pm 10°$ for a 24-h period on the 13–14th; at the same time wind speed was constant within $\pm 5\%$. For more than 48 h on the 16–17th the wind was constant within $\pm 10°$ and $\pm 10\%$. Further, the wind speed changed sufficiently slowly so that we expect the waves to be in quasi-equilibrium.

The LORAN A navigation facility produced 50 μs pulses at 1·95-MHz frequency. The resonant ocean waves are of 77-m wavelength, 7-s period. Each pulse contains about 100 waves, so that the ocean wavelength is selected with a resolution of 1%. The receiver was mounted on a small truck (step van) and driven at uniform speed along the paths indicated in Fig. 3. The path lengths varied from 1·0 to 2·7 km, corresponding to 3 dB beamwidth of the synthesized antenna between 6 and 18°.

The radio data consisted of more than 150 repeated synthetic-aperture measure-

*We assume that recorded hourly averages are in *nautical* miles per hour, which makes them consistent with the instantaneous wind readings. (Weather Bureau records indicate hourly readings of 'miles run' are in *statute* miles, instantaneous winds in knots.) Winds have blown 2 km over land before reaching weather station. Anemometer height is 6·4 m above ground level and 12·8 above sea level. The expected boundary layer thickness is $0{\cdot}37\,(\nu/Ux)^{1/5}\,x = 11$ m for $\nu = 0{\cdot}15$ cm^2 s^{-1}, $U = 10$ m s^{-1} and $x = 2$ km, and so we expect the wind readings to be consistent with an equilibrium terrestrial boundary layer.

ments with a moving receiver, and a lesser amount of data recorded each day with a stationary receiver. The right–left ambiguity was resolved by using a cardoid antenna as the basic receiving element. The main lobe of the cardoid was switched from pulse-to-pulse, alternating from right to left of the direction of travel. This resulted in two

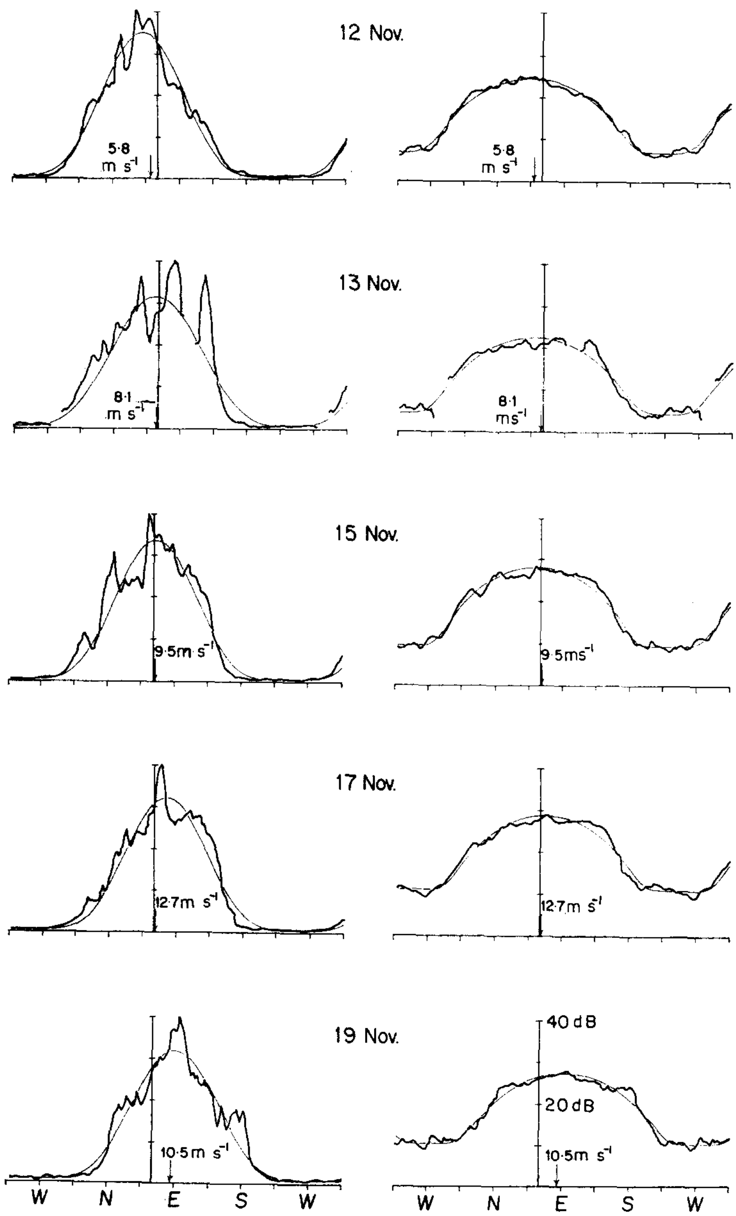

Fig. 6. Directional spectra of approaching 0·14 Hz ocean waves, derived from radio scatter. (Directions follow the wind convention, Fig. 1.) To the left, the energy density is plotted on a linear scale normalized for each day to peak density; to the right, on a logarithmic scale in relative dB units, with the same normalization for the five days. Smooth curves are least-square fits. Wind averages over preceding 8 h are indicated.

simultaneous Doppler spectra from which the right–left ambiguities were removed by least-squares, using the observed antenna response function (measured several times each day, although it was not found to vary).

Records with the receiver stationary shows Bragg peaks at the appropriate frequencies that exceeded second-order scatter by more than 30 dB (Fig. 2). This agrees with first-order scatter theory. Doppler shifts due to currents and other processes were not detectable.

To obtain the smoothed 360° directional spectra (Fig. 6), we combined sequential observations from two headings, separated by only a few minutes in time. Scattered signals from direction within 15° of the vehicle heading were discarded as they are poorly resolved. Spectra were corrected for range attenuation (r^{-4} for ground waves) and an increase in scatter area proportional to r; data from 10 ranges (20·6–88·1km with 7·5-km spacing) and 10 different synthetic-aperture measurements (usually 5 for each heading) observed over a period of several hours, were averaged to reduce statistical fluctuations. These fluctuations are statistical in relation to the long-term behaviour of the sea, but are real in the sense that they represent a narrow-band filtered component of the sea surface during the observing time.

Wave date were recorded by the pitch-and roll buoy for a 3-h period at midday on the 13th and 15th November, about 5 km upwind of the windward shore of the island (Fig. 7).

5. WAVE-DIRECTIONAL MOMENTS

Here we define certain gross moments that can be independently determined by radio scatter and by buoy measurements. The propagation vector **k** has the components (Fig. 1)

$$k_x = k \cos\beta, \quad k_y = k \sin\beta \tag{5.1}$$

in the eastward and northward directions, respectively. Let

$$(\zeta_1, \zeta_2, \zeta_3, \ldots) = (\xi, \partial_x\xi, \partial_y\xi, \ldots) \tag{5.2}$$

designate vertical displacement, components of tilt, and possibly other observables. The spectrum $F_i\,(k_x, k_y)$ of $\zeta_i(x, y;\, t_0)$ at some instant t_0 is so defined that

$$<\zeta_i^2>_{\text{space}} = \int_{-\infty}^{\infty}\int F_i(k_x, k_y)\, dk_x\, dk_y = \int_0^{\infty}\int_0^{2\pi} F_i(k, \beta)\, k\, dk\, d\beta. \tag{5.3}$$

Similarly, for time series $\zeta_i(x, y;t)$ at one point $x_0\, y_0$,

$$<\zeta_i^2>_{\text{time}} = \int_0^{\infty}\int_0^{2\pi} F_i(\omega, \beta)\, d\omega\, d\beta. \tag{5.4}$$

By the ergodic theorem the space and time averages can be equated:

$$F_i(\omega, \beta)\, d\omega = F_i\,(k, \beta)\, k\, dk. \tag{5.5}$$

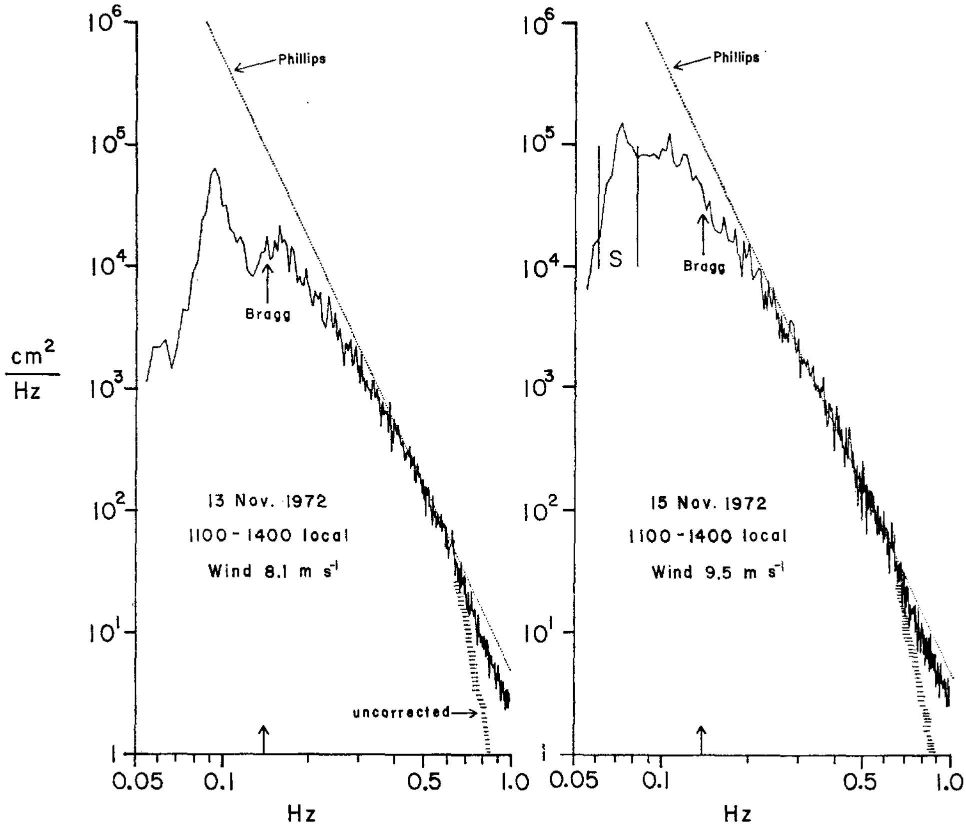

Fig. 7. Wave spectra from buoy accelerometer records, taken 5 km upwind of Wake Island. Raw spectra have been corrected for buoy response (correction is negligible below 0·7 Hz). S identifies a band of swell from 340°T. Arrows at 0·14 Hz indicate Bragg-selected frequencies. The dotted line is the Phillips saturation spectrum, $F(\tilde{\omega}) = Bg^2(2\pi)^{-4}\,\tilde{\omega}^{-5}\,\mathrm{cm^2\,Hz^{-1}}$, $B = 0{\cdot}8 \times 10^{-2}$.

For deep-water waves, $\omega^2 = gk$, and the required Jacobian is

$$J = \frac{F_i(k, \beta)}{F_i(\omega, \beta)} = \frac{1}{k}\frac{\mathrm{d}\omega}{\mathrm{d}k} = \frac{g^2}{2\omega^3}. \tag{5.6}$$

It is convenient to express all measured spectra in terms of $F_1(k_x, k_y)$, $F_1(\omega, \beta)$, etc., e.g. the contributions (per unit wavenumber space, per unit frequency-radian, etc.) to the mean-square surface *elevation*. We omit the subscript '1' and refer to $F(\ )$ as simply the wave spectrum.

The Cartesian moments are written

$$M_{pq} = \int_{-\infty}^{\infty}\int k_x^p\, k_y^q\, F(k_x, k_y)\, \mathrm{d}k_x\, \mathrm{d}k_y = \int_0^{\infty} k^{p+q}\, N_{pq}(k)\, k\, \mathrm{d}k, \tag{5.7}$$

where

$$N_{pq}(k) = \int_0^{2\pi} \cos^p\beta \sin^q\beta \, F(k, \beta)\, d\beta. \tag{5.8}$$

The wave buoy measures the three quantities in equation (2). For an elementary wave train, these are related by

$$\zeta_1 = \xi = Re^{i(\mathbf{k}\cdot\mathbf{x}-\omega t)},$$

$$\zeta_2 = \partial_x\xi = R\, ik \cos\beta \, e^{i(\mathbf{k}\cdot\mathbf{x}-\omega t)},$$

$$\zeta_3 = \partial_y\xi = R\, ik \sin\beta^{i(\mathbf{k}\cdot\mathbf{x}-\omega t)}.$$

The co-spectra C_{ij} and quadrature-spectra Q_{ij} of any pair of quantities ζ_i and ζ_j can be expressed in terms of the moments:

$$\left.\begin{aligned} C_{11}(\omega) &= \int_0^{2\pi} F(\omega, \beta)\, d\beta &&= J^{-1} N_{00}, \\ C_{22}(\omega) &= \int_0^{2\pi} k^2 \cos^2\beta \, F(\omega, \beta)\, d\beta &&= J^{-1} k^2 N_{20}, \\ C_{33}(\omega) &= \int_0^{2\pi} k^2 \sin^2\beta \, F(\omega, \beta)\, d\beta &&= J^{-1} k^2 N_{02}, \end{aligned}\right\} \tag{5.9a}$$

$$\left.\begin{aligned} C_{23}(\omega) &= \int_0^{2\pi} k^2 \cos\beta \sin\beta \, F(\omega, \beta)\, d\beta &&= J^{-1} k^2 N_{11} \\ Q_{12}(\omega) &= \int_0^{2\pi} k \cos\beta \, F(\omega, \beta)\, d\beta &&= J^{-1} k \, N_{10} \\ Q_{13}(\omega) &= \int_0^{2\pi} k \sin\beta \, F(\omega, \beta)\, d\beta &&= J^{-1} k \, N_{01} \end{aligned}\right\} \tag{5.9b}$$

and

$$C_{12} = 0, \; C_{13} = 0, \; Q_{23} = 0. \tag{5.10}$$

Equations (10) express the fact that, for any linear superposition of elementary wave trains, elevation and tilt are in quadrature and the two components of tilt are in phase. In the case of actual data, one hopes that in the spectral matrix

$$\mathscr{S} = \begin{pmatrix} \mathbf{C}_{11} & C_{12} & C_{13} \\ \mathbf{Q}_{12} & \mathbf{C}_{22} & \mathbf{C}_{23} \\ \mathbf{Q}_{13} & Q_{23} & \mathbf{C}_{33} \end{pmatrix} \tag{5.11}$$

the components C_{12}, C_{13}, Q_{23} will be relatively small, as an indication of the goodness of the measurements. Thus the buoy spectra can be interpreted through equations (9) to determine the six **bold** components* in the matrix

$$\mathcal{N} = \begin{pmatrix} \mathbf{N}_{00} & \mathbf{N}_{01} & \mathbf{N}_{02} \\ \mathbf{N}_{10} & \mathbf{N}_{11} & N_{12} \\ \mathbf{N}_{20} & N_{21} & N_{22} \end{pmatrix}. \tag{5.12}$$

But
$$k^2 C_{11} = C_{22} + C_{33}, \text{ or } N_{00} = N_{20} + N_{02}, \tag{5.13}$$

from a trigonometric identity, leaving only five independent moments [equation (13) serves as a consistency check on the buoy observations]. The remaining five moments

$$N_{10}, N_{01}, N_{20}, N_{02}, N_{11} \tag{5.14}$$

are independently derived from the buoy observations in accordance with equations (9a, b).

The same moments are determined by the radio observations. The (dimensionless) scatter cross-section per unit area at the Bragg-selected wavenumber k equals

$$\sigma(k, \beta) = k^4 F(k, \beta), \tag{5.15}$$

according to first-order theory, and it then follows from the definition (8) that

$$N_{pq}(k) = k^{-4} \int_0^{2\pi} \cos^p\beta \sin^q(\beta)\, \sigma(k, \beta)\, d\beta. \tag{5.16}$$

Dividing each of the five moments (14) by N_{00} (e.g. the scalar wavenumber spectrum) separates the problems of relative and absolute calibrations of the radio antenna.

The experimental results are summarized in Tables 1–3. For the radio observations the frequency is Bragg-selected at 0·14 Hz and the independent variable is wind speed and direction. For the buoy observations on a given day the wind is taken as constant, and the independent variable is frequency. In Section 8 the two variables are combined into a single dimensionless parameter μ, essentially a (corrected) wind speed divided by wave velocity; μ can be regarded as a dimensionless wind speed or as a dimensionless wave frequency. The wave spread parameters $s^{(1)}$, $s^{(2)}$, . . . , are defined in (6.8).

The conditions (10) and (13) are reasonably satisfied by the buoy measurements, in the sense that C_{12}, C_{13}, Q_{23} and $C_{22} + C_{33} - k^2 C_{11}$ are in fact relatively small, typically $\pm 5\%$ of the leading terms, and consistent with the statistical uncertainty of the spectral estimates. Table 3 shows the comparison between radio and buoy measurements for the two days when both measurements were made. This is the principal result of our experiment; we regard the agreement as fair.

*That is not to say that N_{12}, N_{21}, N_{22} should be relatively small, but simply that they are not determined by a tilt buoy. They are measured by a 'curvature buoy' which obtains components N_{ij} up to $i + j = 4$ (EWING, 1969).

Table 1. Radio scatter observations of approaching 0·14 Hz *ocean waves.*

	12 *Nov.* 72 1152–1602*	13: 1103–1307	14: 1054–1428	14: 1438–1617	15: 0915–1100	15: 1108–1308	16: 1215–1540	17: 1105–1410	18: 1050–1355	19: 1140–1518
Wind† (m s^{-1})	5·8	8·1	9·4	9·5	9·0	9·5	13·1	12·7	10·7	10·5
	50 °T	60	62	63	68	62	60	62	92	87
μ	0·045	0·069	0·083	0·084	0·078	0·084	0·124	0·120	0·097	0·095
Relative power	1·19	0·74	2·44	2·05	2·55	2·61	3·30	3·02	4·76	2·31
Directional moments										
N_{10}/N_{00}	−0·41	−0·47	−0·66	−0·66	−0·56	−0·59	−0·60	−0·62	−0·59	−0·62
N_{01}/N_{00}	−0·49	−0·38	−0·43	−0·45	−0·32	−0·21	−0·35	−0·19	0·01	0·02
N_{20}/N_{00}	0·47	0·51	0·58	0·57	0·55	0·59	0·55	0·58	0·53	0·56
N_{02}/N_{00}	0·53	0·49	0·42	0·43	0·45	0·41	0·45	0·42	0·47	0·44
N_{11}/N_{00}	0·08	0·03	0·20	0·22	0·05	0·00	0·10	0·02	−0·04	0·01
Linear fit										
°T_0	39	57	57	54	63	75	60	75	93	90
α‡	0·020	—	0·020	0·024	—	0·024	—	0·003	—	0·012
s	4·2	2·8	10·7	12·8	3·6	4·0	4·7	3·8	2·8	3·5
Residual(%)	1·6	6·1	2·2	1·6	3·0	6·7	1·1	2·4	2·5	2·6
Logarithmic fit										
°T_0	45	48	60	60	54	57	60	66	84	93
α‡	0·017	0·016	0·012	0·008	0·013	0·026	0·007	0·016	0·013	0·021
s	4·5	4·4	9·4	7·9	5·0	4·9	6·0	5·0	3·4	4·6
Residual (%)	0·4	1·3	1·2	0·7	0·7	1·8	0·7	0·8	0·4	0·8

*Local time.
†Averaged over 8 h prior to mid-record.
‡Blank entries correspond to negative α.

Table 2. Wave-directional moments and associated factors, from buoy observations.

	1972, 13 *November** 1040–1325 *local, wind* 8·1 m s^{-1} *from* 60°T						
Frequency (Hz)	0·147†	0·244	0·342	0·439	0·536	0·635	0·732‡
μ	0·07	0·12	0·16	0·21	0·25	0·30	0·36
Power (cm^2 Hz^{-1})	14,000	3630	896	311	109	46	18
N_{10}/N_{00}	−0·60	−0·60	−0·57	−0·49	−0·46	−0·38	−0·25
N_{01}/N_{00}	−0·28	−0·38	−0·37	−0·36	−0·30	−0·30	−0·23
N_{20}/N_{00}	0·64	0·56	0·56	0·48	0·52	0·50	0·46
N_{02}/N_{00}	0·39	0·42	0·46	0·45	0·49	0·52	0·59
N_{11}/N_{00}	−0·01	0·10	0·08	0·06	0·01	0·01	0·05
°T$_0$	63	58	57	54	57	52	52
$s^{(1)}$	3·9	4·8	4·2	3·1	2·5	1·9	1·0
$s^{(2)}$	5·3	5·0	4·4	3·6	2·4	2·4	4·1
$s^{(3)}$	1·9	4·6	4·3	4·1	2·3	1·7	0·7
$s^{(4)}$	39·8	8·1	5·9	3·4	2·7	1·1	0·1
	1972, 15 *November*§ 1121–1344 *local, wind* 9·5 m s^{-1} *from* 62°T						
Frequency (Hz)	0·147	0·244	0·342	0·439	0·536	0·635	0·732
μ	0·09	0·14	0·20	0·26	0·32	0·38	0·43
Power (cm^2 Hz^{-1})	40,500	5520	1190	341	113	49	17
N_{10}/N_{00}	−0·58	−0·53	−0·42	−0·42	−0·34	−0·26	−0·13
N_{01}/N_{00}	−0·32	−0·45	−0·43	−0·35	−0·32	−0·26	−0·21
N_{20}/N_{00}	0·57	0·50	0·47	0·51	0·50	0·47	0·50
N_{02}/N_{00}	0·39	0·48	0·50	0·51	0·56	0·54	0·52
N_{11}/N_{00}	+0·04	0·11	0·08	−0·01	−0·07	−0·07	−0·11
°T$_0$	67	50	47	50	48	45	33
$s^{(1)}$	3·9	4·6	3·5	2·4	1·7	1·2	0·7
$s^{(2)}$	4·3	4·8	3·8	2·1	3·7	3·9	4·7
$s^{(3)}$	2·8	5·1	4·0	1·9	1·0	0·7	0·2
$s^{(4)}$	12·5	3·4	1·0	2·0	0·2	—	10·2

*Resolution 0·098 Hz, 2048 degrees of freedom.
†Bragg frequency is at 0·14 Hz.
‡Buoy cut-off frequency at 0·7 Hz.
§Resolution 0·098 Hz, 1408 degrees of freedom.

6. BEAM PARAMETERS

LCS have shown that the pitch-and-roll buoy may be regarded as a directional antenna with 88° beam width [though one can do somewhat better from the knowledge that $F(k, \beta)$ is always positive]. This compares to a resolution of 6° for our best radio scatter runs. Accordingly, the procedure adopted was to derive the directional spectrum (and some of its moments) from the radio scattering method, the buoy serving as an independent check of five gross moments so derived.

The high angular resolution of the radio scatter method enables us to test various models of directional distribution. The most satisfactory model turned out to be a modified LCS pattern

$$G(\theta) = \alpha + (1-\alpha)g(\theta), \quad g(\theta) = \cos^s(\tfrac{1}{2}\theta), \quad \theta = \beta - \beta_0, \tag{6.1}$$

Table 3. Comparison of radio scatter with buoy observations. The wave-directional moments and associated factors are for approaching 0·14-Hz *ocean waves. Bandwidth for buoy analysis is* 0·098 Hz, *for radio analysis* 0·001 Hz.

	13 *Nov.* 1972, *wind* 8·1 m s^{-1} *from* 60°T $\mu = 0{\cdot}069$		15 *Nov.* 1972, *wind* 9·5 m s^{-1} *from* 62°T $\mu = 0{\cdot}084$	
	Radio	*Buoy*	*Radio*	*Buoy*
Local time	1103–1307	1040–1325	1108–1308	1121–1344
Relative power	1·0	1·0	3·5	2·9
N_{10}/N_{00}	−0·47	−0·60	−0·59	−0·58
N_{01}/N_{00}	−0·38	−0·28	−0·21	−0·32
N_{20}/N_{00}	0·51	0·64	0·59	0·57
N_{02}/N_{00}	0·49	0·39	0·41	0·39
N_{11}/N_{00}	0·03	−0·01	−0·00	+0·04
°T$_0$	57°T/48°T*	63	75/57	67
s	2·8/4·4*	3·9/5·3/1·9†	4·0/4·9	3·9/4·3/2·8

*The two radio values correspond to linear/logarithmic fitting.
†The three buoy values correspond to $s^{(1)}/s^{(2)}/s^{(3)}$.

where $G(\theta)$ decreases monotonically from

$$G = 1 \text{ at } \theta = 0 \text{ to } G = \alpha \text{ at } \theta = \pm\pi. \tag{6.2}$$

[If $s > 1$, then $\partial_\theta G(\theta) = 0$ at $|\theta| = \pi$, thus avoiding a kink at the minimum.] The normalization is

$$H(s) = \int_{-\pi}^{\pi} G(\theta)d\theta = 2\pi\alpha + (1-\alpha)\, L(s), \quad L(s) = 2\pi^{\frac{1}{2}}\Gamma(\tfrac{1}{2}s+\tfrac{1}{2})/\Gamma(\tfrac{1}{2}s+1). \tag{6.3}$$

The computed scatter cross-section is now written

$$\hat{\sigma}(k, \theta) = k^4\hat{F}(k, \beta),\ \hat{F}(k, \beta) = \Phi(k)\, G(\theta;\, \beta_0, s, \alpha)/H(s), \tag{6.4}$$

and the parameters Φ, β_0, s, α are evaluated by minimizing

$\int_{-\pi}^{\pi} [\sigma(\theta) - \hat{}(\theta)]^2\, d\theta$, thus leaving a relative residual

$\int_{-\pi}^{\pi} [\sigma(\theta) - \hat{\sigma}(\theta)]^2\, d\theta \Big/ \int_{-\pi}^{\pi} \sigma^2(\theta)\, d\theta$. The procedure is repeated, substituting $\log \sigma$, $\log \hat{\sigma}$

for σ, $\hat{\sigma}$. The linear fitting emphasizes the spectrum near its peak; the logarithmic fitting allows for the fact that spectral uncertainties are in a fixed *ratio* to the true values.

The results are shown in Fig. 6. Table 1 gives the day-to-day variation in power Φ (relative units), the wave direction $°T_0 = -\beta_0 - \frac{1}{2}\pi$, the wave spread s, the 'anti-wind' component α, and the per cent residuals. The derived directions generally follow the wind direction, with better agreement for logarithmic fittings. The residuals are small (Table 1), of the order of 1% for the logarithmic fittings, a few per cent for the linear fittings; in part they are the expected result of statistical fluctuation. Values of α are of order 10^{-2}. (These might be experimental error; if so, they indicate an upper limit.) Since α is small, $G(\theta) = \cos^s(\frac{1}{2}\theta)$ is an adequate representation except near $\theta = 180°$; for small θ, $\cos^s(\frac{1}{2}\theta)$ is close to $\cos^{s/4}\theta$, and so the traditional $\cos^2\theta$ corresponds to $s = 8$ (a rather large value).

$°T_0$ and s can be evaluated from the buoy observations. It is convenientto use the Fourier expansion $G(\theta) = \cos^s(\frac{1}{2}\theta) = [\frac{1}{2}(1+\cos\theta)]^{s/2} = L\pi^{-1}\sum_{j=0} c_j \cos j\theta$,

$$c_0, c_1, c_2, \ldots c_j = \frac{1}{2}, \frac{s}{s+2}, \frac{s(s-2)}{(s+2)(s+4)}, \ldots \frac{\varepsilon_j}{2} \frac{\Gamma^2(\frac{1}{2}s+1)}{\Gamma(\frac{1}{2}s+1+j)\Gamma(\frac{1}{2}s+1-j)}, \tag{6.5}$$

where $\varepsilon_0 = 1$ and $\varepsilon_j = 2$ for $j = 1, 2 \ldots$ For $s = 2, 4, \ldots$ the series terminates at $j = 1, 2, \ldots \frac{1}{2}s$. Using this expansion in $F(k, \beta) = \Phi(k)\, G(\theta)/H$ and substituting into (5.8) leads to

$$\begin{bmatrix} N_{00} \\ N_{10} \\ N_{01} \\ N_{20} \\ N_{02} \\ N_{11} \end{bmatrix} = \Phi \begin{bmatrix} 1 \\ 0 \\ 0 \\ \frac{1}{2} \\ \frac{1}{2} \\ 0 \end{bmatrix} + \frac{\Phi(1-\alpha)L}{H} \begin{bmatrix} 0 \\ c_1\cos\beta_0 \\ c_1\sin\beta_0 \\ \frac{1}{2}c_2\cos 2\beta_0 \\ -\frac{1}{2}c_2\cos 2\beta_0 \\ \frac{1}{2}c_2\sin 2\beta_2 \end{bmatrix}. \tag{6.6}$$

The integrated power is $N_{00} = \Phi$. The principal wave direction is consistent with either of the forms

$$\tan\beta_0 = \frac{N_{01}}{N_{10}} \text{ or } \tan 2\beta_0 = \frac{2N_{11}}{N_{20}-N_{02}}, \tag{6.7}$$

and the wave spread s can be evaluated from any of the expressions

$$\begin{aligned} R^{(1)} &= \frac{(N_{10}^2+N_{02}^2)^{\frac{1}{2}}}{N_{00}} &&= c_1 f(\alpha, s^{(1)}) \\ R^{(2)} &= \pm\frac{[(N_{20}-N_{02})^2+4N_{11}^2]^{\frac{1}{2}}}{N_{00}} &&= c_2 f(\alpha, s^{(2)}) \\ R^{(3)} &= \frac{N_{10}\,N_{01}}{N_{00}\,N_{11}} &&= \frac{c_1^2}{c_2} f(\alpha, s^{(3)}) \\ R^{(4)} &= \frac{N_{10}^2-N_{01}^2}{N_{00}\,(N_{20}-N_{02})} &&= \frac{c_1^2}{c_2} f(\alpha, s^{(4)}) \end{aligned} \tag{6.8}$$

with
$$f(\alpha, s) = \left[1 + \frac{2\pi\alpha}{(1-\alpha)\, L(s)}\right]^{-1}$$

a small correction factor. [*LCS* use the r.h.s. of (6.7) for direction and $R^{(2)}$ for beam width. The l.h.s. of CARTWRIGHT (1963) equation (17) corresponds to $R^{(1)}$ and the r.h.s. to $R^{(2)}$, respectively.]

We have used the l.h.s. of (6.7) to obtain ${}^{\circ}T_0$, and have calculated $s^{(j)}$ from $R^{(j)}$ in (6.8), setting $\alpha = 0$. In the expression for $R^{(2)}$ the negative root is taken when $s < 2$. $R^{(4)}$, $s^{(4)}$ are poorly determined since they depend on a difference between moments. Values of $s^{(j)}$ are plotted in Fig. 8. Table 3 gives the comparison between beam

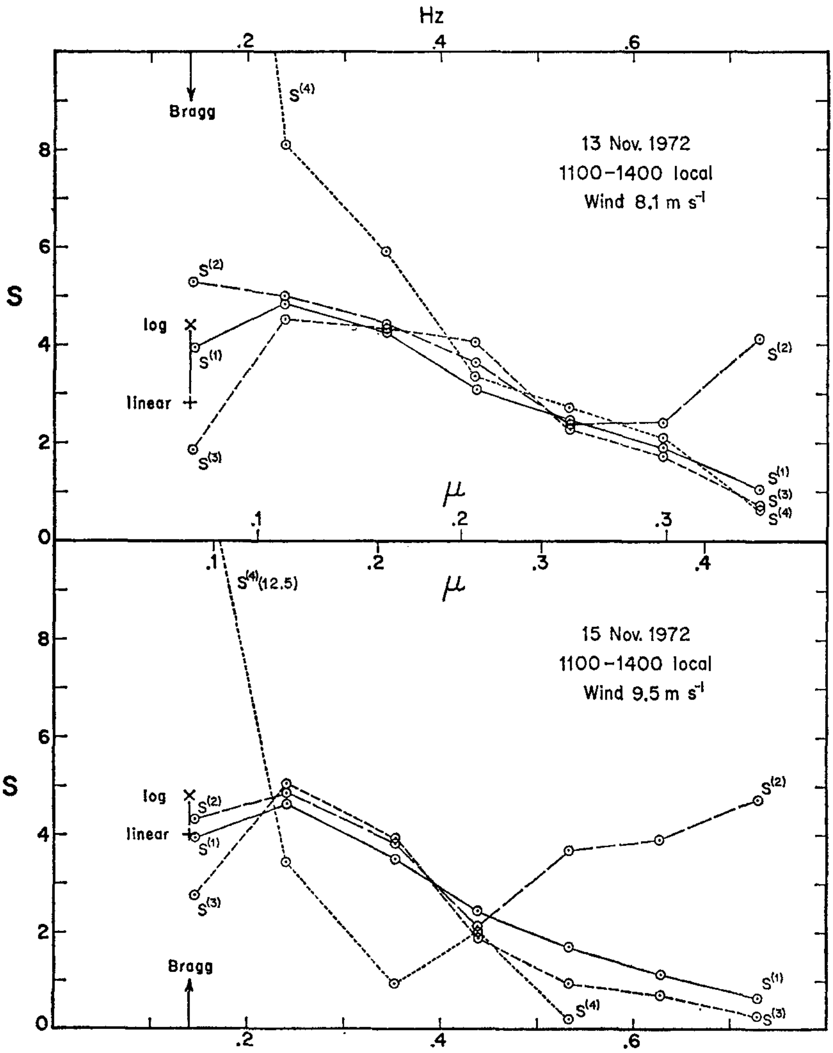

Fig. 8. Wave spreads from buoy motion, ⊙ [equation (6.8)], and from radio scatter at 0·14 Hz (linear fit +, logarithmic fit ×).

parameters from radio scatter and wave buoy. The internal consistency between the various s values is an indication of the validity of the assumed $G(\theta)$ model. At both high and low frequencies, $s^{(2)}$ (which involves second moments) exceeds $s^{(1)}$ and $s^{(3)}$ (derived from first moments). In general, the values for 13 November exceed those for 15 November. The results became compatible when plotted against the frequency parameter μ that allows for the difference in wind speed (section 9).

The N_{ij} derived from the radio data can be used in the same manner as the buoy data to calculate $s^{(j)}$ using (6.8). The values so calculated (not shown) have a scatter similar to the $s^{(j)}$ derived from the buoy data.

7. EQUILIBRIUM AND SATURATION

A central concept in the geophysical discussion is the idealization of a fully developed (aroused) sea; the associated spectra are referred to as equilibrium spectra. The concept goes back to oceanographic antiquity, but the prerequisite balance of generating and dissipating fluxes is not yet understood. Still, for some given wind conditions and some specific frequency, the power density eventually attains a steady value, more quickly at high frequencies than at low frequencies.

We may read off some very rough estimates from the empirical curves of PIERSON, NEUMANN and JAMES (1955):

	at 0·14 Hz		
Wind (m s⁻¹)	t_{min} (h)	x_{min} (km)	$\tilde{\omega}_{sat}$ (Hz)
5	3	22	0·26
10	7	92	0·13
15	10	140	0·09

Wind speed refers to 'anemometer level', 10 m, say. If the wind duration exceeds t_{min} *and* if the fetch exceeds x_{min}, then the power density at 0·14 Hz has reached equilibrium; it does not increase with increasing time and fetch. The storm fetches greatly exceed x_{min} (Fig. 4). With regard to duration, we regard t_{min} as closely related to the generation time of the 0·14-Hz waves, and accordingly interpret the wave observations with wind averages over the preceding 8 h.

The last column gives the 'roll-off' frequency of the spectrum. For an equilibrium sea ($t > t_{min}$, $x > x_{min}$), frequencies above $\tilde{\omega}_{sat}$ are *saturated:* the energy densities do not increase with increasing wind. Thus 0·14-Hz waves should be saturated for winds above 10 m s^{-1}.

The relative power from radio scatter (Table 1) is not consistently larger at 13 m s^{-1} than at 10 m s^{-1}, in accord with the foregoing considerations. The buoy observations give higher energy densities for 9·5 m s^{-1} compared to 8·1 m s^{-1} winds at frequencies below 0·5 Hz (see also Fig. 7), but the discrepancy becomes pronounced only below 0·25 Hz. The foregoing PNJ values suggest a lower saturation frequency, ω_{sat} = 0·17 Hz at 8·5 m s^{-1}. We conclude that the Wake Island sea was barely saturated at 0·14 Hz during the highest winds.

8. THE μ-PARAMETER

To compare measurements under different wind conditions, and to remove the anemometer level as a variable, it is convenient to plot the data as a function of a parameter

$$\mu = \frac{u_*/\kappa}{c}, \tag{8.1}$$

where $u_* = (\tau/\rho)^{\frac{1}{2}}$ is the so-called 'friction velocity' and $\kappa = 0{\cdot}4$ is von Karman's constant. $c = g/\omega = g/(2\pi\bar{\omega})$ is wave velocity. We assume the anemometer to be within the logarithmic layer, $u(z) = (u_*/\kappa)\ \ln z/z_0$, we calculate u_0 from the observed value of u at elevation z by further assuming that

$$z_0 = \Omega u_*^2/g\kappa^2, \tag{8.2}$$

where $\Omega/\kappa^2 \approx 0{\cdot}0156$ is Charnock's constant.* Alternatively, we could calculate u_* from a knowledge of the drag coefficient

$$\gamma^2 = \tau/\rho u^2 \tag{8.3}$$

where τ is surface stress. For the logarithmic profile and the value $\Omega/\kappa^2 = 0{\cdot}0156$, and using

$$\gamma = u^*/u = \kappa/ln\ z/z_0, \tag{8.4}$$

one obtains the following numerical values:

	$u^* =$	10	20	30	40	50 cm s^{-1}
	$z_0 =$	0·0016	0·0064	0·0143	0·0255	0·040 cm
$z = 6{\cdot}4$ m (*Wake Island anemometer*)						
	$u =$	3·22	5·75	8·03	10·13	12·10 m s^{-1}
	$\gamma^2 =$	0·00096	0·0012	0·0014	0·0016	0·0017
$z = 10$ m						
	$u =$	3·33	5·98	8·37	10·58	12·6 m s^{-1}
	$\gamma^2 =$	0·00090	0·0011	0·0013	0·0014	0·0016

We note that for the assumed Charnock constant, γ^2 remains within the customary limits 10^{-3} to 2×10^{-3} over a wide range of wind speeds. (Wu sets $\gamma^2 = 2{\cdot}6 \times 10^{-3}$ for $u > 15$ m s^{-1}.)

The discussion is similar to that given by LCS. At the least we regard μ as a convenient way to correct for anemometer height (provided this is within the loga-

*The numerical value is not critical; the foregoing choice is based on a recent compilation of field and laboratory observations by WU (1969). Charnock's original value was 0·0112. LHS took 0·0812 (hence $\Omega = 0{\cdot}013$)! We have converted their measurements as follows: from their Fig. 12 (record 5) one obtains $u_* = g\kappa\mu/\sigma = 53$ cm^{-1}, and $u(10\text{ m}) = 11$ m s^{-1}, assuming $\Omega/\kappa^2 = 0{\cdot}0812$ and a ship's anemometer height of 10 m. Converting backwards with $\Omega/\kappa^2 = 0{\cdot}0156$ yields $u_* = 43$ cm^{-1}, and $\mu = \mu_{LCS} \times 43/53$. Thus even with this extreme variation in Charnock's constant, the results are not qualitatively changed.

rithmic layer). A bolder interpretation relates μ to the momentum flux across the air–sea boundary.

Plotting the spread measurements as function of μ (Fig. 9) brings the buoy measurements for the two days into accord; they are also in reasonable accord with the (adjusted) LCS buoy experiment. The trend of $s(\mu)$ is reasonably defined in the range $0{\cdot}125 < \mu < 0{\cdot}3$. Above $\mu = 0{\cdot}3$ our $s^{(2)}$ values (but not those of LCS) are inconsistent with $s^{(1)}$ and $s^{(3)}$. In all events there is a breakdown of any consistency at $\mu = 0{\cdot}1$; below 0·075 (say) a value something like $s = 4$ (dashed line) is indicated. We suggest that below $\mu = 0{\cdot}075$, and possibly above $\mu = 0{\cdot}3$, processes other than wind-generation (e.g. the nonlinear transfer processes) are significantly involved. In fact (as a reviewer has emphasized), recent work associated with JONSWAP (Hasselmann *et al.*, 1973) has demonstrated the role of nonlinearities at *all* frequencies, and so our reliance on a wind-based parameter and associated angular scaling θ_r (below) may be misplaced.

9. RESONANCE ANGLE

Phillips (1957) introduced the notion of a resonance angle, θ_r, so defined that the wind-component in the direction of wave travel equals the wave velocity, $u \cos\theta_r = c$.

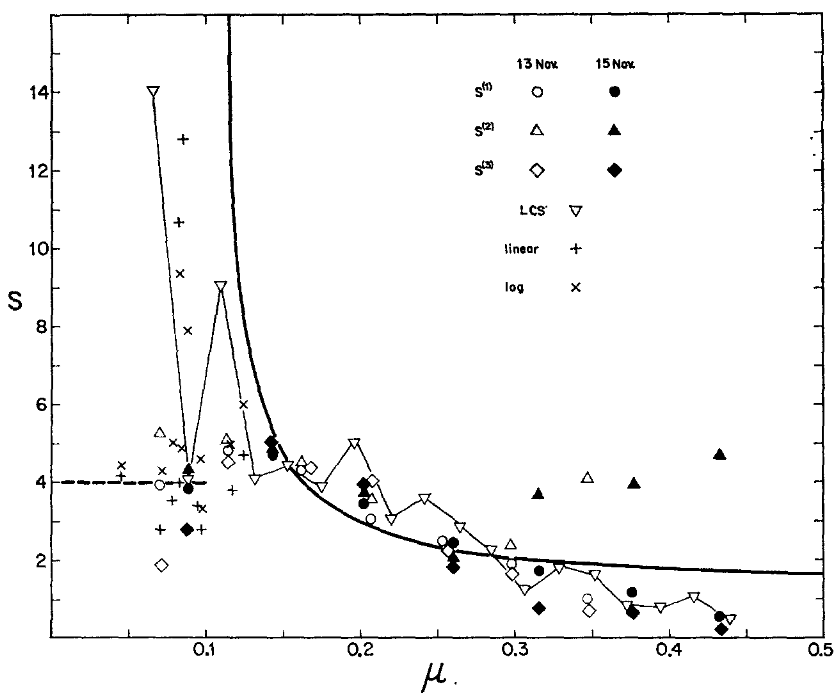

Fig. 9. Summary plot of wave spread. Our buoy measurements are shown by open symbols for 13 November and solid symbols for 15 November. The LCS measurements (downward-pointing triangle) are connected by a thin line. The radio measurements are indicated by + and ×, respectively. The heavy curve corresponds to the relation (9·4) with parameters (9·5).

The coalescence of data in Fig. 9 requires that we take u at height related to wavelength, $z_w = A/k$, with A = order (1). Using $k = g/c^2$,

$$\sec\theta_r = \mu \ln (A\,\Omega^{-1}\,\mu^{-2}). \tag{9.1}$$

Setting $\theta_r = 0$ defines a cutoff value* for μ:

$$1 = \mu_0 \ln (A\Omega^{-1}\,\mu_0{}^{-2}) \tag{9.2}$$

and associated cutoff parameters,

$$\omega_0 = \frac{g\kappa\mu_0}{u_*},\ c_0 = \frac{u_*}{\kappa\mu_0}. \tag{9.3}$$

Thus the choice of A uniquely determines μ_0.

For $\Omega = 0{\cdot}0025$, we have

$\mu_0 =$	0·10	0·093	0·083
$A =$	0·55	1	π

and for $u_* = 50$ cm s^{-1}, $u_{10\text{ m}} = 12{\cdot}6$ m s^{-1},

$\tilde{\omega}_0 =$	0·125	0·116	0·103	Hz
$c_0/u_{10\text{ m}} =$	0·99	1·07	1·20.	

This associates the usual cutoff frequency† (below which the waves outrun the wind) with $\theta_r \to 0$, the point of view taken by PHILLIPS (1966, p. 128).

One can relate the spread s to the resonance angle θ_r. For resonance excitation, $g(\theta)$ consists of two beams at $0 = \pm\theta_r$. Wind gusting and nonlinear interactions can be expected to fill out the beam between $\pm\theta_r$, leading to a weekly bimodal distribution (as claimed by GILCHRIST, 1966), or possibly wipe out the resonance double beam altogether, as indicated by the scatter measurements. In all events we expect the beam to be weak well beyond $|\theta_r|$, and have some relative power such as $g(\theta_r) = \frac{1}{2}$ or $\sqrt{2}/2$ at the resonance angle. Combining the previous results we have then (neglecting α)

$$g(\theta_r) = \cos^s(\tfrac{1}{2}\theta_r),\ \sec\theta_r = \mu \ln (A\Omega^{-1}\,\mu^{-2}), \tag{9.4}$$

which can be solved for $s(\mu)$. As $\mu \to \mu_0$, $s \to \infty$; and as $\mu \to \infty$, $\theta_r \to 90°$, and $s \to \log g(\theta_r)/\log \cos 45°$. We select $g(\theta_r) = \sqrt{2}/2$, so that $1 < s < \infty$, thus avoiding a

*A second root $\mu = \sqrt{(A/\Omega)} \approx 15$ corresponds to capillary frequencies, well beyond the scope of this discussion.

†An alternate approach is to define a parameter $\gamma = kz_c/\Omega$ based on the critical height z_c, defined by $u(z_c) = c$. This gives $\gamma = \mu^2 e^{1/\mu}$, with a minimum of 1·85 at $\mu = \frac{1}{2}$. At the cutoff frequency μ_0, $kz_c = \gamma\Omega = A$. There are then two equivalent ways of interpreting the low-frequency cutoff: (i) that for $\mu < \mu_0$ the winds within a wavelength of the surface are too slow relative to the wave velocity, or (ii) that the critical height is too large relative to the wavelength.

kink at $\theta = \pi$ [equation (6.3)]. Further we select $\mu_0 = 0{\cdot}1$, and this leads to the curve in Fig. 9. We readily admit that this choice of parameters

$$g(\theta_r) = \sqrt{2}/2,\ \mu_0 = 0{\cdot}1 \tag{9.5}$$

is highly arbitrary, and reminds one of the 'oceanographic level' agreement claimed by the original $\cos^2\theta$ beam pattern [equation (1.1)].

10. SOME DERIVED PROPERTIES

The $\cos^s(\frac{1}{2}\theta)$ model can be used to derive some interesting relations. Cox and Munk (1954a, b) have measured the slope statistics from the glitter of sun, and obtain a value of about 2 for the ratio of upwind to crosswind components of mean-square slope. The two components are

$\int_0^\infty \int_0^{2\pi} k^2 \begin{bmatrix}\cos^2\theta \\ \sin^2\theta\end{bmatrix} F(k, \beta)\, k\, d\beta\, dk$. Converting to $F(\mu, \theta) = \Phi(\mu) \cos^s(\frac{1}{2}\theta)/L(s)$,

$\Phi(\mu) = B\kappa^{-4}u_*^4 g^{-2}\mu^{-5}$ for $\mu \geq \mu_0$ and zero otherwise, the components are [using the expansion (6.5)]

$$B \int_{\mu_0}^{\mu} \frac{\mu^{-1}}{L(s)}\, d\mu \int_{-\pi}^{\pi} \begin{bmatrix}\cos^2\theta \\ \sin^2\theta\end{bmatrix} \cos^s(\tfrac{1}{2}\theta)\, d\theta = \tfrac{1}{2}B \int_0^x I^{\pm}\, dx \tag{10.1}$$

$$I^{\pm} = 1 \pm \frac{s(s-2)}{(s+2)(s+4)}, \quad s = \frac{\ln\frac{1}{2}}{\ln\left[\frac{1}{2} + \frac{1}{2}\,\frac{e^{-x}}{1-2\mu_0 x}\right]}, \tag{10.2}$$

where $$x = \ln(\mu/\mu_0).$$

The two slope components have equal spectral density at $\mu = 3{\cdot}13\ \mu_0 = 0{\cdot}313$; at higher frequencies the crosswind components actually exceed the up/down wind components (Fig. 10). The ratio of mean-square slope components depends strongly on the upper limit, and this might be set by capillarity (and is then wind-dependent). It appears as if the computed ratio is smaller than observed.

The monitoring of pressure fluctuations on the deep-sea bottom could provide some further information on the directional spectrum. Near the surface the wave-induced pressure fluctuations diminish exponentially with depth, eventually reaching a level that depends on the product of nearly oppositely-traveling wave trains (partially standing waves). This second-order effect has been extensively studied (Longuet-Higgins, 1950; Hasselmann, 1963) in its relation to the generation of microseisms. The pressure spectrum on the sea floor is given by (Hasselmann, 1963)

$$F_p(\vec{k}, 2\omega) = \tfrac{1}{2}\rho^2 g^2 \omega \int_{-\pi}^{\pi} F(\omega, \theta)\, F(\omega, \theta+\pi)\, d\theta. \tag{10.3}$$

Note that F_p is identically zero for the PNJ spectrum (1.1).

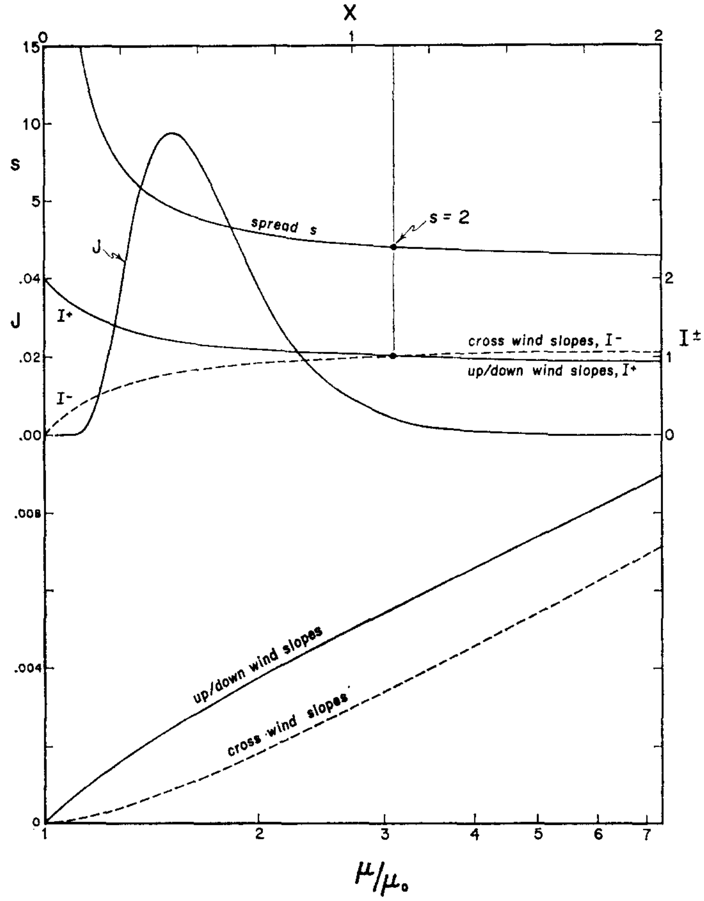

Fig. 10. Slope components plotted against $x = \ln(\mu/\mu_0)$. Top: the spread factor $s(\mu)$ according to (9·4); Center: the $I\pm$ curves [equation (10.2)] are proportional to the spectral densities of the slope components, the J-integral [equation (10.7)] to the spectral density of 'standing wave' components. Bottom: cumulative mean-square slope components between 0 and x [equation (10.2)].

Writing $F(\omega, \theta) = \Phi(\omega)\, G(\theta)/H$

$$F_p(\vec{k}, 2\omega) = \tfrac{1}{2}\rho^2 g^2 \omega\; \Phi^2(\omega) H^{-2}\, I,\; I = \int_{-\pi}^{\pi} G(\theta)\; G(\theta+\pi)\; d\theta. \tag{10.4}$$

Again we can set $\alpha = 0$ without appreciable error (thus $H = L$, $G = g$), the important contributions coming from waves travelling near-perpendicular to the wind; allowing for the symmetry relation $g(\theta) = g(-\theta)$,

$$I(s) = \int_{\pi}^{\pi} [\cos\tfrac{1}{2}\theta \cos\tfrac{1}{2}(\pi-\theta)]^s\, d\theta = 4\int_0^{\pi/2} [\tfrac{1}{2}\sin\theta]^s\, d\theta = 2^{1-s}\, \pi^{\frac{1}{2}}\, \frac{\Gamma(\frac{1}{2}s+\frac{1}{2})}{\Gamma(\frac{1}{2}s+1)}. \tag{10.5}$$

The mean-square elevation is

$$<\xi^2> = \int_{\omega_0}^{\infty} \Phi(\omega)\, d\omega = \int_{\omega_0}^{\infty} Bg^2\omega^{-5}\, d\omega = \tfrac{1}{4}Bg^2\omega_0^{-4}$$

and $$F_p(\vec{k}, 2\omega) = 8\rho^2 g^2 <\xi^2>^2 (\omega/\omega_0)^{-9}\, \omega_0^{-1}\, I(s)/L^2(s). \tag{10.6}$$

The k-integration has an upper limit* of the order $k_0 = 2\omega/C_S$ where C_S is sound velocity, and so for an isotropic pressure field

$$F_p(2\omega) = \int_0^{k_0}\int_{-\pi}^{\pi} F_p(\vec{k}, 2\omega)\, k\, dk\, d\theta = 32\pi\rho^2 g^2 <\xi^2>^2 C_S^{-2}\, \omega_0(\omega/\omega_0)^{-7}\, I(s)/L^2(s). \tag{10.7}$$

Integrating now over frequency, and using the expression for $<\xi^2>$,

$$\int_{\omega_0}^{\infty} F_p\,(2\omega)\, d\omega = \rho^2 g^2 <\xi^2>\, KJ,\;\; J = \int_0^{\infty} 8\pi^{\frac{1}{2}} \frac{e^{-6x}\, 2^{-s}\, \Gamma(\frac{1}{2}s+1)}{\Gamma(\frac{1}{2}s+\frac{1}{2})}\, dx, \tag{10.8}$$

where $K = B^{\frac{1}{2}}g <\xi^2>^{\frac{1}{2}} C_S^{-2} \approx 3\times 10^{-7}$ r.m.s. (ξ m) is a dimensionless parameter, and $x = ln\,(\mu/\mu_0) = ln\,(\omega/\omega_0)$, with $s(x)$ given by (10.2). The J-integrand is plotted in Fig. 10. The maximum contribution comes from $\mu = 1{\cdot}51\ \mu_0$. At smaller values of μ the integrand is small because so little wave energy spreads beyond $\theta = \pm 90°$; at larger μ because the total wave energy (and even more so $<\xi^2>^{3/2}$) diminishes so rapidly with frequency. By numerical integration we find $J = 0{\cdot}0375$. For comparison, in the case of two opposite pencil beams, we have $G(\theta) = \delta(\theta) + \delta(\theta + \pi)$, $H = 2$, $H^{-2}I = \frac{1}{2}$, giving $J = \pi/4$. The r.m.s. bottom pressure equals the r.m.s. 'surface pressure' $\rho g <\xi^2>^{\frac{1}{2}}$ times $(KJ)^{\frac{1}{2}}$. For r.m.s. $\xi = 1$ m, $(KJ)^{\frac{1}{2}} = 1{\cdot}06 \times 10^{-4}$, and the r.m.s. deep pressure fluctuations are 10^{-2} mbar.

In the case $u_* = 50$ cm s^{-1} ($u_{10\,m} = 12{\cdot}6$ m s^{-1}), we found $\tilde{\omega}_0 = 0{\cdot}125$ Hz. Thus the J-integrand has a maximum at $1{\cdot}51\ \tilde{\omega}_0 = 0{\cdot}19$ Hz, and the microseism spectrum is peaked at twice this frequency, in accord with 3-s microseisms reported by HAUBRICH and MCCAMY (1969) from open-sea storms (as opposed to coastal microseisms). But there is good evidence that such microseisms are related to interference between waves from different storm sectors, whereas we have treated the case of a unidirectional fetch.

11. FINE-STRUCTURE

So far the scatter cross-sections have been averaged over many range bins and over many successive runs. In this way the cross-sections have been smeared into a broad, smooth distribution. There is some interest as to whether narrow peaks found in individual range bins for short periods of time can be interpreted as narrow beams imbedded in the broad pattern.

Figure 11 has been so plotted that any features moving towards the island at the

*We are indebted to the reviewer for pointing out an incorrect procedure in the original manuscript.

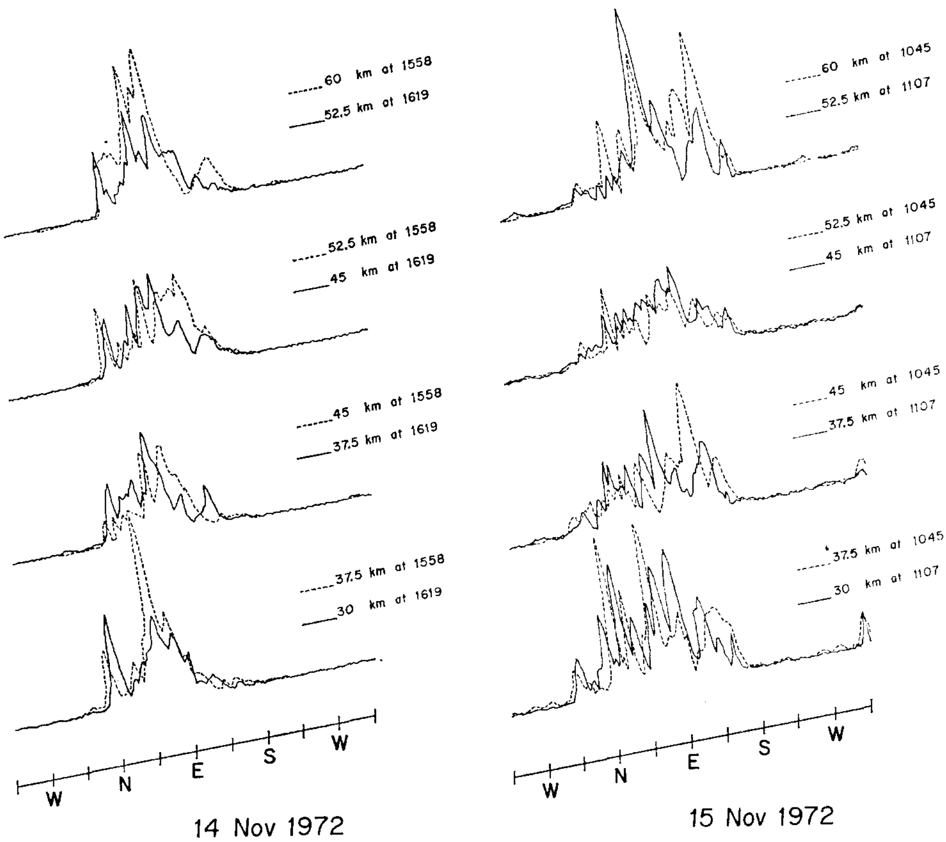

Fig. 11. Directional spectra for individual range bins centered at distances of 60, 52·5, .. 30 km from the island. For each spectral pair, the dashed curve refers to an earlier time t_1 and a more distant range r_1, the solid curve to t_2, r_2, with a time interval t_2–t_1 ($\approx$ 22 min) so chosen that the Bragg-selected approaching waves move at group velocity from r_1 to r_2 in an interval t_2–t_1. The plots are linear in power and drawn to the same scale.

appropriate group velocity would show up in the superimposed solid and dashed curves, these being displaced in distance and time so that the ratio

$$\frac{r_1-r_2}{t_2-t_1} \approx \frac{g}{2\omega} = 19{\cdot}6 \text{ km h}^{-1}$$

equals the group velocity. Some common features can in fact be found, but the evidence is marginal. A similar analysis for larger time intervals (t_3-t_1, t_4-t_1, . .) between more distant range bins (r_1-r_3, r_1-r_4, . .) showed no correlation.

Under the assumption of homogeneity, a narrow beam would have shown up continuously in *all* range bins pointing in the appropriate direction. This appears not to be the case. The simplest interpretation of peaks in fine-structure is to assume a peak in overall energy (at the Bragg line) in a particular scatter bin at a particular time. We observe the portion radiated towards the island within the resolution bandwidth $\delta\varphi$, but the total directional spread can be broader. The fact that such a wave packet cannot be followed beyond adjacent range bins would suggest that local generation and dissipation processes are significant over a distance of 15 km, or that the narrow beam is sufficiently rotated by currents so that it is no longer visible.

12. DISCUSSION

The improvement (by factor of 10) in angular resolution of the radio scatter measurements as compared to the pitch-and-roll measurements has not led to any significant revisions. Evidently the wind-generated sea is broad, without reproducible fine-structure.

For the winds encountered at Wake Island, the LORAN radio source happens to be in Bragg resonance with ocean waves near the low-frequency cutoff, where the directional pattern varies rapidly with wind speed. This does not prevent a comparison between the radio and buoy measurement (though it strains it because of inevitable differences between the two methods in forming space and time averages).

The directional spread just above the cutoff frequency is much narrower than below cutoff frequency, and the transition is sharp. Presumably the narrow-beam higher frequencies are wind-dominated, and the wide-beam lower frequencies are dominated by nonlinear transfer processes. This is consistent also with a remark by J. A. Ewing (personal communication) that frequency components in process of rapid growth subtend a narrower beam than after they attain equilibrium.

Our work was motivated in part by an effort to use radio scatter from ocean waves for remotely sensing surface winds. For consistent results one will want to work comfortably (but not too far) above the cutoff frequency. The following table lists the range of desirable ocean radio wave frequencies at two selected wind speeds:

	$u^* = 20$ cms^{-1}, $u_{10\,m} = 6$ m s^{-1}			$u^* = 50$ cm s^{-1}, $u_{10\,m} = 12{\cdot}6$ m s^{-1}		
μ	0·15	0·25	0·35	0·15	0·25	0·35
Ocean waves (Hz)	0·47	0·78	1·09	0·19	0·31	0·44
Radio waves (MHz)	21·2	58·5	114	3·47	9·24	18·6

For ionospheric transmissions, frequencies between 14 and 20 MHz appear favorable.

Acknowledgement—This work has been supported by the Advanced Research Projects Agency of the Department of Defense and was monitored by the Office of Naval Research under Contract No. N00014-69-A-0200-6012.

REFERENCES

ARTHUR R. S. (1949) Variability in direction of wave travel. Ocean surface waves. *Annals of the New York Academy of Sciences*, **51**, 511–522.

BARBER N. F. (1949) A diffraction analysis of a photograph of the sea. *Nature*, **164**, 485.

BARBER N. F. (1959) A proposed method of surveying the wave state of the open ocean. *New Zealand Journal of Science*, **2**, 99–108.

BARRICK D. E. (1972) *Remote sensing of the troposphere*, V. DERR, editor, U.S. Government Printing Office, Chapter 12, 12–1 to 12–46.

CARTWRIGHT D. E. (1963) The use of directional spectra in studying the output of a wave recorder on a moving ship. In: *Ocean wave spectra*, Prentice-Hall, Englewood Cliffs, N.J., pp. 203–218.
CHASE J., L. J. COTE, W. MARKS, E. MEHR, W. J. PIERSON, JR., F. G. RÖNNE, G. STEPHENSON, R. C. VETTER and R. G. WALDEN (1957) The directional spectrum of a wind generated sea as determined from data obtained by the Stereo Wave Observation Project, New York University, College of Engineering, Department of Meteorology and Oceanography and Engineering Statistics Group, Technical Report, ONR Contract Nonr 285(03), 267 pp. (Unpublished manuscript.)
COX C. S. and W. H. MUNK (1954a) Measurement of the roughness of the sea surface from photographs of the sun's glitter. *Journal of the Optical Society of America*, **44**, 838–850.
COX C. S. and W. H. MUNK (1954b) Statistics of the sea surface derived from sun glitter. *Journal of Marine Research*, **13**, 198–227.
CROMBIE D. D. (1955) Doppler spectrum of sea echo at 13·56 Mc/s. *Nature*, **175**, 681–682.
EWING J. A. (1969) Some measurements of the directional wave spectrum. *Journal of Marine Research*, **27**, 163–171.
GILCHRIST A. W. R. (1966) The directional spectrum of ocean waves: an experimental investigation of certain predictions of the Miles–Phillips theory of wave generation. *Journal of Fluid Mechanics*, **25**, 795–816.
HASSELMANN K. (1963) A statistical analysis of the generation of microseisms. *Reviews of Geophysics*, **1**, 177–210.
HASSELMANN K., T. P. BARNETT, E. BOUWS, H. CARLSON, D. E. CARTWRIGHT, K. ENKE, J. A. EWING, H. GIENAPP, D. E. HASSELMANN, P. KRUSEMAN, A. MEERBURG, P. MULLER, D. J. OLBERS, K. RICHTER, W. SELL and H. WALDEN (1973) Measurements of wind-wave growth and swell decay during the Joint North Sea Wave Project (JONSWAP). *Ergänzungsheft zur Deutschen Hydrographischen Zeitschrift*, Reihe A(8°), Nr. 12, 95 pp.
HAUBRICH R. A. and K. MCCAMY (1969 Microseisms: coastal and pelagic sources. *Reviews of Geophysics*, **7**, 539–571.
KINSMAN B. (1965) *Wind waves—their generation and propagation on the ocean surface*, Prentice-Hall, 676 pp.
LONGUET-HIGGINS M. S. (1950) A theory of the origin of microseisms. *Philosophical Transactions of the Royal Society* A, **243**, 1–35.
LONGUET-HIGGINS M. S., D. E. CARTWRIGHT and N. D. SMITH (LCS) (1963) Observations of the directional spectrum of sea waves using the motions of a floating buoy. In: *Ocean wave spectra*, Prentice-Hall, pp. 111–136.
PHILLIPS O. M. (1957) On the generation of waves by turbulent wind. *Journal of Fluid Mechanics*, **2**, 417–445.
PHILLIPS O. M. (1966) *The dynamics of the upper ocean*, Cambridge University Press (reprinted with corrections 1969), 261 pp.
PIERSON W. J., JR., G. NEUMANN and R. W. JAMES (PNJ) (1955) Practical methods for observing and forecasting ocean waves by means of wave spectra and statistics. *Publications. U.S. Navy Hydrographic Office* No. 603 (reprinted 1960), 284 pp.
SAENGER R. A. (1969) Measurement of the statistical properties of the ocean surface with instrumental surface floats—Part II. Engineering and data processing. New York School of Engineering and Science, Geophysical Sciences Laboratory Technical Report TR-69-10. (Unpublished manuscript.)
STILWELL D., JR. (1969) Directional energy spectra of the sea from photographs. *Journal of Geophysical Research*, **74**, 1974–1986.
SUGIMORI Y. (1973) Dispersion of the directional spectrum of short gravity waves in the Kuroshio Current. *Deep-Sea Research*, **20**, 747–756.
TEAGUE C. C., G. L. TYLER, J. W. JOY and R. H. STEWART (1973) Synthetic aperture observations of directional height spectra for 7 s ocean waves. *Nature, Physical Sciences*, **244**, 98–100.
WU J. (1969) Wind stress and surface roughness at air–sea interface. *Journal of Geophysical Research*, 74, 444–455.